Draft version August 30, 2022
Typeset using LaTeX **manuscript** style in AASTeX62

arXiv:2208.02493v2 [astro-ph.SR] 28 Aug 2022

Do Cellular Automaton Avalanche Models Simulate the Quasi-Periodic Pulsations of Solar Flares?

Nastaran Farhang,[1] Farhad Shahbazi,[1] and Hossein Safari[2]

[1]*Department of Physics, Isfahan University of Technology, 84156-83111, Isfahan, Iran*

[2]*Department of Physics, Faculty of Science, University of Zanjan, 45195-313, Zanjan, Iran*

ABSTRACT

Quasi-periodic pulsations (QPPs) with various periods that originate in the underlying magnetohydrodynamic processes of the flaring structures are detected repeatedly in the solar flare emissions. We apply a 2D cellular automaton (CA) avalanche model to simulate QPPs as a result of a repetitive load/unload mechanism. We show that the frequent occurrence of magnetic reconnections in a flaring loop could induce quasi-periodic patterns in the detected emissions. We obtain that among 21,070 simulated flares, 813 events endure over 50 seconds, scaled with the temporal resolution of the Yohkoh Hard X-ray Telescope, and about 70% of these rather long-lasting events exhibit QPPs. We also illustrate that the applied CA model provides a wide range of periodicities for QPPs. Furthermore, we observe the presence of multiple periods in nearly 50% of the cases applying the Lomb-Scargle periodogram. A lognormal distribution is fitted to the unimodal distribution of the periods as a manifestation of an underlying multiplicative mechanism that typifies the effect of the system's independent varying parameters. The global maximum of the periods' lognormal distribution is located at 29.29 ± 0.67 seconds. We compare statistics of the simulated QPPs with parameters of the host flares

Corresponding author: Nastaran Farhang
farhangnastaran@gmail.com

safari@znu.ac.ir

and discuss the impacts of flare properties on QPPs' periods. Considering the intrinsic characteristic of CA models, namely the repetitive load/unload mechanism, and the obtained pieces of evidence, we suggest that CA models may generate QPPs. We also examine the applicability of the autoregressive integrated moving average models to describe the simulated and observational QPPs.

1. INTRODUCTION

Quasi-periodic pulsations (QPPs) with periods ranging from a few seconds to several minutes are often observed across the entire flare emissions, synchronously (Dennis 1985; Nakariakov & Melnikov 2009; Van Doorsselaere et al. 2016; Dominique et al. 2018; Nakariakov et al. 2018; Hayes et al. 2019; Zimovets et al. 2021). The understanding of QPPs and their underlying physical mechanism has been subject to many studies in recent decades (see McLaughlin et al. 2018, for a recent review). In general, QPPs are believed to be generated by either propagation and dissipation of MHD modes in the solar corona (i.e., oscillatory processes) or an underlying load/unload mechanism (i.e., self-oscillatory processes). Each mechanism involves individual characteristics for these modulated patterns.

The main idea of the oscillatory processes is that small perturbations in plasma parameters (e.g., magnetic field strength, temperature, etc.) produce magnetohydrodynamic (MHD) waves. The evanescence of MHD waves modulates the plasma emissions, namely QPPs occur. Various models have been developed to investigate different oscillatory modes as possible candidates for energy modulations (e.g., Nakariakov et al. 2004; Nakariakov & Verwichte 2005; Chen & Priest 2006; Nakariakov et al. 2006; Nakariakov & Melnikov 2009; De Moortel & Nakariakov 2012; Takasao & Shibata 2016; Dennis et al. 2017). According to this perspective, all MHD modes can modulate microwave emissions. The longitudinal and torsional modes could not describe the simultaneous modulation of microwave and HXR bands. Nevertheless, sausage and kink modes could produce synchronized modulation across the entire electromagnetic spectrum. These models are capable of producing a wide range of periodicities as well as describing multiple periods observed in

QPPs (Nakariakov et al. 2003; Melnikov et al. 2005; Van Doorsselaere et al. 2011; Hong et al. 2021; Lu et al. 2021).

In self-oscillatory processes, the system is governed by a cyclical mechanism in which energy accumulates as a power supply (e.g., photospheric motions) slowly and continuously derives the system. If the free energy exceeds some threshold, the system releases a significant amount of energy through an avalanche process. In this context, the QPPs are triggered as a result of the frequent occurrence of magnetic reconnections which modulates the released energy and the acceleration of charged particles. The load/unload mechanism could describe synchronous emissions at different wavelengths (Aschwanden 1987; Craig & McClymont 1991; Ofman & Sui 2006; Zaitsev & Stepanov 2008; McLaughlin et al. 2012a,b; Hayes et al. 2016; Li et al. 2020).

Despite many theoretical and observational studies, it is yet unclear whether QPPs are derived by restoring forces in the perturbed coronal plasma, or they are direct outputs of repetitive reconnection regimes. It is also possible that each of these mechanisms effectively plays a role. Statistical analysis of oscillatory parameters and their governing scaling laws could practically provide information about the formation of QPPs. In addition to theoretical modeling and data analysis, numerical studies may provide a different and new approach to interpret QPPs.

Taking the idea of self-oscillatory processes into account, we perform a numerical study to simulate and investigate the statistics of QPPs. For this purpose, we consider solar flares as a self-organized critical (SOC) system and apply a modified version of the Lu & Hamilton (1991) model to numerically reproduce magnetic relaxations (flare-like events) and their accompanying QPPs. The remainder of this paper is organized as follows: In Section 2, we argue the possibility of simulating QPPs as a result of a load/unload mechanism by cellular automaton (CA) models. Then, we introduce the characteristics of the applied model in Section 3. We describe the detection of QPPs in the numerical modeling in Section 4. We also present the statistics of simulated QPPs and compare them with observational reports. In Section 5, we briefly review some classes of linear processes applicable in time series modeling and investigate their productivity in examining both simulated and observational QPPs. Finally, we conclude in Section 6.

2. IS IT TECHNICALLY POSSIBLE TO SIMULATE QPPS BY CA MODELS?

By definition, the natural tendency of a system to automatically adjust its components to establish a critical state is called SOC, provided that exceeding some threshold leads to scale-free fluctuations in the system (Aschwanden 2011). In the SOC mechanism, a gradual energy supply drives the system towards a critical state at which it relaxes through a sequence (avalanche) of nonlinear energy-dissipative events. The frequency-size distribution of released energies manifests a power-law-like behavior. The threshold is an intrinsic feature of SOC and the driving timescale is much larger than the avalanche timescale.

SOC was introduced by Bak et al. (1987) who established the first CA avalanche model, namely the sand-pile model. The model employs a grid with nodal values representing the sand distribution in the system. The initial state is constructed using random numbers and the energy supply mechanism operates as grains gradually drop into randomly selected sites, which builds up local piles. In the case of exceeding a critical slope in the system, the sand grains fall off the unstable pile to reduce the slant and relax the system. Since the driving operation time is negligible compared to the avalanche timescale, in numerical modeling the driving mechanism halts once an instability occurs and automatically reactivates after the release of the free energy. Hence, the energy balance is maintained in the SOC systems. The CA approach provides the ability to investigate the complex behavior of avalanche processes by breaking them down into smaller pieces.

The scale-free distribution of solar flare energies evokes the application of SOC models to study the stochastic nature of these events (Georgoulis & Vlahos 1998; Wheatland 2001; Charbonneau et al. 2001; Wheatland & Litvinenko 2001; Nita et al. 2002; Wheatland 2008; Morales & Charbonneau 2008, 2010; Mendoza et al. 2014; Dănilă et al. 2015; Farhang et al. 2018; Alipour et al. 2019; Najafi et al. 2020). Solar flares occur due to a gradual and continual increase of magnetic stress in the solar atmosphere. The coronal magnetic field evolves as magnetic structures emerge, twist, braid, or annihilate on the Sun's surface, and relaxes through e.g., magnetic reconnections. Local relaxations may raise the stress elsewhere in the system and lead to a sequence of reconnections with massive release of energy (Gold & Hoyle 1960; Forbes 1991; Longcope 1996; Biskamp 2000;

Priest & Forbes 2000; Somov 2010; Loureiro & Uzdensky 2016). As a result of the energy load and unload cycle, coronal magnetic topology changes. The stored magnetic energy converts to heat (e.g., ohmic dissipation) and kinetic energy of charged particles (generating MHD oscillatory modes, shock waves, and turbulence in the plasma). Therefore, various physical processes trigger thermal (EUV and SXR) and non-thermal (e.g., microwave, HXR, etc.) emissions during a solar flare (Carmichael 1964; Sturrock 1968; Hirayama 1974; Kopp & Pneuman 1976; Somov 1991; Svestka & Cliver 1992; Somov & Kosugi 1997; Fletcher et al. 2011; Priest 2014; Benz 2017). These emissions are often associate with QPPs.

Parker (1988) proposed that gradual perturbations in the solar atmosphere lead the coronal magnetic structures towards an unstable state. Hence, small bursts (magnetic reconnections) occur as the building blocks of flaring events. Accordingly, Lu & Hamilton (1991) introduced a lattice-based model to investigate the efficiency of the CA approach in simulating solar coronal explosive events. Lu and Hamilton defined a discrete magnetic field over a 3D grid of nodes and applied a driving mechanism for topological evolution of the solar magnetic field. In the constructed model, the stressed magnetic field relaxes along with a series of magnetic reconnections, after which the system dives into a new equilibrium state. The frequency-size distribution of simulated flaring events is shown to follow a power law.

Based on the above discussion, CA models are technically adequate for simulating QPPs by a load/unload mechanism since they are well capable of reproducing repetitive reconnection regimes. Here, we use a modified version of the Lu & Hamilton model in two dimensions and reassess its outputs and their physical interpretations. In our simulation, instead of a magnetic field we define a magnetic vector potential field over a 2D grid. Therefore, the magnetic field remains divergence-free over time. The model is introduced in detail in the next section.

3. MODEL PROPERTIES

We consider a 2D lattice as a cross-section of a coronal loop and study the variation of the magnetic field inside this sector. Uniformly distributed random numbers are used to construct the initial state. The nodal values represent the magnetic vector potential field, $\mathbf{A} = A(x, y)\hat{z}$ in which $\hat{z}$ is a unit

vector along the loop axis. We also consider the open boundary condition by keeping $A = 0$ on borders. This allows the energy to leak out of the system's boundaries. Otherwise, there will be an exponential growth in the energy and the system could never reach a stable state.

To imitate the evolution of the coronal magnetic field, a local driving mechanism is applied. Therefore, a small disturbance, generated from a uniform distribution, is added to an arbitrary node at each *driving step*. Then, the stability of the entire system is checked through the criterion:

$$|\Delta A_{i,j}| \equiv \left| A_{i,j} - \frac{1}{4}\sum_{l=1}^{4} A_l \right| > A_c, \tag{1}$$

where the sum runs over the four nearest neighbors (A_l). The instability threshold, A_c, is a random number generated from a Gaussian distribution with e.g., $\mu = 1$ and $\sigma = 0.01$. Should the instability criterion fulfil anywhere in the system, the field locally relaxes through a set of redistributions:

$$\begin{aligned} A_{i,j}^{n+1} &= A_{i,j}^{n} - \frac{4}{5}A_c, \\ A_{l}^{n+1} &= A_{l}^{n} + \frac{1}{5}A_c, \end{aligned} \tag{2}$$

where n denotes the *evolution step*, $A_{i,j}$ is the central node, and $l = 1, 2, 3, 4$.

In this perspective, a magnetic reconnection is regarded as short-range interactions between an unstable node and its nearest neighbors. A succession of redistributions from an inceptive instability somewhere to ultimate stability everywhere is called an avalanche (flare). Various choices of redistribution rules are possible including conservative or nonconservative, isotropic or anisotropic, and deterministic or probabilistic. Also, long-distance interactions are conceivable (see: Isliker et al. 1998; Charbonneau et al. 2001; Strugarek et al. 2014; Farhang et al. 2018, 2019).

There are two different aspects in measuring the constructed configuration's energy: the lattice energy and the released energy. The development of the former should expectedly demonstrate an energy balance in the system as the implemented open boundary condition avoids a continuous increase of energy. Therefore, the system reaches an approximate stationary state on top of which the energy fluctuates due to excitements and relaxations. Besides exhibiting a power-law-like behavior, the latter could provide important information about the underlying physical mechanisms.

In a magnetic configuration, the energy is proportional to the square of the magnetic field strength. Therefore, we have:

$$E_{\rm latt} \propto \sum_{\rm lattice} B^2 \propto \sum_{\rm lattice} |\nabla \times \mathbf{A}|^2 \propto \sum_{\rm lattice} A^2. \tag{3}$$

The matter of interest is to appraise the ability of CA models in generating QPPs. An extensive understanding of the energy release process is required to achieve this purpose. The amount of released energy during each redistribution is:

$$e_{i,j} = \sum \left(A^{n+1}\right)^2 - \sum \left(A^n\right)^2 = \frac{4}{5}\left(1 - 2\frac{|\Delta A_{i,j}|}{A_c}\right) A_c^2, \tag{4}$$

where the sum runs over the five nodes engaged in the redistribution.

Since there is no preferred direction in the system, all unstable nodes are redistributed simultaneously. One can consider it as a bunch of reconnecting events occurring in a single *time frame*. Therefore, the total released energy during each frame is:

$$e_{frame} = \sum e_{i,j}, \tag{5}$$

and the sum includes all the identified unstable nodes.

Local redistributions may cause other instabilities in the system. Thus, the system's stability needs to be examined again after each time frame. In the case of appearing new instabilities in the system, the whole "check-redistribute" procedure continues until an equilibrium is achieved. Then, the driving mechanism operates again. Accordingly, the flare energy is the sum of the released energies in successive frames between two driving steps or equivalently the energy difference between two consecutive driving steps:

$$E_{\rm flare} = \sum e_{frame} \simeq E_{\rm latt}^{t+1} - E_{\rm latt}^{t}, \tag{6}$$

where t denotes the driving step.

4. NUMERICAL QPPS AND THEIR PERIODICITIES

We established a square lattice of magnetic vector potential field with $\mathbf{256 \times 256}$ grids and studied its evolution over $200,000$ driving steps. Figure 1 shows the variation of the lattice energy during

which 20 million, 275 thousand, 220 magnetic reconnections occurred in the system. Starting from an initially random state, it took over 4 million evolution steps for the system to reach an approximate stationary state over which the energy fluctuates around a constant average value. We restrict our study to the total number of 21,070 flaring events registered after the energy balance is delivered to the system (i.e., 124,064 driving steps or equivalently 15,677,989 evolution steps).

4.1. *QPPs in CA Models*

We propose that the released energies during individual frames can be considered as the energy recorded by solar detectors within their temporal resolution. Hence, the released/detected energy from a flaring event is supposed to exhibit a quasi-periodic pattern (as a representation of QPPs). Figure 2 displays an example of the detected QPPs for a simulated flare with the total dimensionless energy of 5.74×10^4, in which 61,834 magnetic reconnections occurred during 884 frames.

For comparison, the observed emissions of a solar flare recorded by the Yohkoh satellite are presented in Figure 3. The subject flare occurred on March 1th, 1998 at 17:09 and lasted over 10 minutes. The Yohkoh Hard X-ray Telescope (HXT) registered this event in four spectral bands (i.e., L, M1, M2, and H bands) with a temporal resolution of half-seconds. The attended oscillatory patterns are referred to as QPPs.

One important question is whether all registered energies within consecutive frames in both observations and simulations exhibit quasi-periodic characteristics. Inglis et al. (2016) conducted an extensive study on several M and X flares recorded by the Geostationary Operational Environmental Satellite (GOES) and the Gamma-ray Burst Monitor (GBM). They found that roughly one-third of the studied flares were attended by quasi-oscillatory patterns. Furthermore, Szaforz & Tomczak (2019) investigated the partially occulted flares listed in the Yohkoh Legacy Data Archive (YLA) and determined that less than 50% of these emissions exhibit QPPs. Failure to detect QPPs in a large fraction of observations might be due to limited sensitivity of the instruments, deficiency of computational methods, inappropriate interpretation of QPPs, or the absence of these pulsations along with flaring events. In the following, we assess the likelihood of numerical QPPs representing similar statistics. But first, we introduce the algorithm used to study the periodicities.

4.2. *The Lomb-Scargle Periodogram*

The Lomb-Scargle periodogram is a powerful mathematical tool developed to study the oscillatory parameters in data samples. Having its origins in the Fourier transform, this periodogram decomposes a discrete regular/irregular signal (S) to its independent frequency components:

$$\mathcal{P}_S = \frac{1}{2}\left(\frac{[\sum_j S_j \cos\omega(t_j-\tau)]^2}{\sum_j \cos^2\omega(t_j-\tau)} + \frac{[\sum_j S_j \sin\omega(t_j-\tau)]^2}{\sum_j \sin^2\omega(t_j-\tau)} \right), \tag{7}$$

where the sum includes all data samples and $\mathcal{P}_S$ is the estimate of the power spectral density (PSD). The parameter τ,

$$\tan(2\omega\tau) = \frac{\sum_j \sin 2\omega t_j}{\sum_j \cos 2\omega t_j}, \tag{8}$$

guarantees the orthogonality of the sinusoidal terms in Equation (8) and equips the algorithm to be invariant under global time shifts, in contrast to the fast Fourier transformation (Lomb 1976; Scargle 1982).

By some means, the Lomb-Scargle periodogram is equivalent to other frequency analysis techniques, namely the least-square fitting, phase-folding, and Bayesian methods (VanderPlas 2018). It also provides a χ^2-distributed power spectrum for Gaussian uncertainties (Vio et al. 2013). Due to its convenient properties, the Lomb-Scargle periodogram has a widespread application in time series analysis particularly in astronomical studies (e.g., Tarnopolski & Marchenko 2021; Zhang et al. 2021; Saikia et al. 2022). Here, we apply this technique to study the numerical QPPs' periodicities.

Once the analysis is performed, the significance level of each frequency component is validated against the "false alarm probability" (FAP). The FAP estimates the likelihood of a frequency to appear in the periodogram due to the existence of noise in the signal rather than the original source. Various methods have been developed to measure the FAP in presence of different contaminative sources (Horne & Baliunas 1986; Baluev 2008; Delisle et al. 2020a,b). In the simplest case, the FAP is measured assuming a white noise in the time series, whilst in the more complicated contexts correlated noise are considered.

Figure 4 shows an example of a PSD obtained for the observational QPPs together with the FAP significance levels of $50, 10, 1$, and 0.01 percent. To identify the dominant frequencies in the power

spectrum, we use a Gaussian filter:

$$F(\mathcal{P},\nu) = H(\nu)\exp\left(-\frac{\mathcal{P}-C(\nu)^2}{W(\nu)^2}\right), \tag{9}$$

where H, W, and C are the height, width, and contribution of each peak in the PSD. We also filter out the harmonics. Further details of the applied frequency extraction technique are discussed in the next section.

4.3. *Statistics of the Simulated flares and QPPs*

Applying the CA approach, 21,070 flares are simulated with dimensionless energies of 0.7 to 2.4×10^5. Figure 5 displays the probability distribution functions (PDFs) of the simulated flare energies and lifetimes (durations, D). Expectedly, both distributions exhibit power-law-like behaviors (Lu & Hamilton 1991; Charbonneau et al. 2001). The simulated events are categorized into 5 types (labeled as A, B, C, M, and X flares) relevant to the GOES classification system. Among all events, only 813 flares (about 3.8%) released their energy in more than 100 frames. Therefore, considering the liberated (free) energies in consecutive frames analogous to emissions recorded by the HXT in half-seconds intervals, most of the flares lasted less than 50 seconds. The simulated events with $D > 50$ seconds are mostly C-class and above. Durations less than 50 seconds may also relate to small-scale flaring events such as small-scale brightenings (microflares, campfires, bright coronal points, etc.) that have been recently observed with space missions (see e.g., Chen et al. 2021; Berghmans et al. 2021; Shokri et al. 2022).

As shown in Figure 5, both distributions are fitted with power-law functions. For the energy distribution the power index is 1.45 ± 0.02 and the goodness-of-fit is assessed using the Kolmogorov-Smirnov test (KS-test). The KS-test gives a measure of the departure between two distributions based on a decision-making routine (between a null and an alternative hypothesis). It also returns a $p-$value that validates the decision. In this case, the null hypothesis is that the PDF follows a power law and the obtained $p-$value, 0.98, does not reject the null. This power-law (scale-free) behavior suggests that the CA self-oscillatory processes can be considered as the generative mechanism of self-similar, self-organized or self-organized criticality. It also implies that magnetic reconnections

are most probably the leading generator of flaring events (Parker 1988; Aschwanden 2011). For the duration distribution, the power-law function exhibits a better match with the significant events (the tail of the distribution) rather than the small-scale events with energies < B0-class, including A-class flares and other tiny features. The power index is 1.71 ± 0.02 with $p-$value of 0.90. The obtained $p-$value indicates that the difference between the PDF and the power-law function is not statistically significant.

To perform a cyclical analysis, usually, the first step is to normalize the subject time series. Various forms of normalization are possible (Ogasawara et al. 2010; Panigrahi & Behera 2013). Here, we apply two common types and argue their effects on the PSDs. The applied normalization routines are:

$$S_N = \frac{S - \bar{S}}{\bar{S}}, \tag{10}$$

$$S_{MA} = \frac{S - \hat{S}_k}{\hat{S}_k}, \tag{11}$$

where $\bar{S}$ is the overall mean value of S and $\hat{S}_k$ is the moving average over a window with size k. In the remaining of this paper, S_N and S_{MA} are referred to as normalized and smoothed time series, respectively.

Figure 4 displays the PSDs obtained for the HXR emissions of a solar flare recorded by Yohkoh together with the FAP levels. The FAP provides an estimation of the accuracy of the extracted periods. Hence, we only consider periods with intensities higher than 0.01% significance level (the green horizontal line) as true findings. The top panels of the figure are the results of applying the Lomb-Scargle periodogram on the smoothed times series with $k = 80$. The most prominent peaks of the PSDs are located at $22.24, 21.83$, and 27.48 seconds for L, M1, and M2 bands, respectively. No significant peak is obtained for the H band. The bottom panels correspond to the normalized time series. In contrast with the smoothed time series that most likely have one prominent peak, the PSDs of normalized light curves might manifest more peaks. However, the extracted periods of the smoothed samples are highly sensitive to the averaging window size and various choices of k do not reproduce convergent results. Therefore, Equation (10) provides a more reliable normalization

(without any information loss), particularly in cyclical analysis. We apply Equation (10) to the registered energies and evaluate their periodicities. We include all the peaks above the maximum FAP level in the performed survey.

Figure 6 illustrates an example of the obtained PSDs for a few of simulated flares. As seen in the figure, the power spectrums exhibit a power-law-like behavior in the log-frequency presentation. Such a statistic of the PSD have been previously reported in the solar and stellar studies including observations of solar flares and QPPs (e.g., Cenko et al. 2010; Gruber et al. 2011; Ireland et al. 2014; Inglis et al. 2016). This result also attests to the productivity of the CA approach in the reproduction of flares and QPPs.

We investigate the properties of the simulated QPPs in two regimes of $D \leq 50$ and $D > 50$ seconds. Figure 7 displays the histograms (number) of extracted periods for both regimes individually (panels a & b) and collectively (panel c). Among $20,257$ events of the first regime, about 36% of flares lasted long enough (more than 5 frames) to perform the frequency analysis. Our analysis shows that, less than 1% of these flares are accompanied by QPPs. However, in the seconds regime ($D > 50$), quasi-periodic patterns are observed in nearly 70% of events. We observe that about 47%, 41%, and 12% of QPPs exhibit $1, 2$, and 3 conspicuous peaks in their PSDs, respectively. We fit a lognormal distribution to the unimodal histograms of Figure 7. The lognormal distribution is,

$$L(p, \mu, \sigma) = \frac{1}{p\sigma\sqrt{2\pi}} \exp\left(\frac{-(\ln(p) - \mu)^2}{2\sigma^2}\right), \tag{12}$$

where μ and σ are the scale and shape parameters, respectively. The global maximum of the fitted lognormal distribution is:

$$Mode[p] = e^{\mu - \sigma^2}, \tag{13}$$

which represents the most probable period of the simulated QPPs and equals to 33.66 ± 0.71 and 29.29 ± 0.67 seconds for panels (b) and (c), respectively. Applying the KS-test, the $p-$values are also obtained 0.56 and 0.62, respectively.

It is well known that, the lognormal distribution is a characteristic of stochastic systems that associate with the multiplicative effect of independent varying parameters (Mitzenmacher 2004; Tokovinin

2014; Ruocco et al. 2017). Therefore, the obtained lognormal distribution for the periodicities might originate in the driving mechanism, the number of unstable sites contributing to reconnections, or even the amount of released energies. One may ask how two different generative mechanisms i.e., the power-law behavior (Figures 5 and 6) and the lognormal behavior (Figure 7) may work together in a system. Pauluhn & Solanki (2007) developed a stochastic model for generating small-scale flaring emissions with an initial power-law distribution that evolved via random kicks as a multiplicative process. In such a system, although the time series develops due to a multiplying generative mechanism, the inceptive power-law behavior of the event distribution is stored in the memory of the time series. The machine learning methods have been applied to determine the power-law index of such simulated and observational time series (e.g., Bazarghan et al. 2008; Tajfirouze & Safari 2012; Sadeghi & Safari 2019; Upendran & Tripathi 2021).

Valdivia et al. (2005) argued that intermittent SOC phenomena (e.g., reconnections and substorms) and self-similar turbulent plasma sheets present power-law characteristics. Furthermore, Alipour et al. studied the morphological and intensity structures of the small-scale brightenings (campfires) observed by the Solar Orbiter. They discussed that, to some extent, both the power law and lognormal functions could conveniently model the heavy-tailed distributions of campfires' duration, peak intensity, and size. Moreover, they showed that small-scale brightenings mainly occur at the supergranular cell boundaries (Figure 7, therein). Therefore, these features are analogous to flaring events in the sense of an underlying generative mechanism (i.e., magnetic reconnections), except that they appear in much smaller scales. In other words, one may consider QPPs, or even campfires, related to the reconnection regimes that occur between adjacent magnetic structures as the magnetic field sweeps towards the footpoints via horizontal or turbulent flows. For further discussion on power laws and multiplicative processes see Thurner et al. (2018), section 3.3.3 therein.

Evaluating the existence of any statistical relationship between the oscillatory parameters of the QPPs and the host flares could provide intuition about the underlying generative mechanism. Here, we assess the dependency of the simulated QPPs' periods on the host flare durations and energies. Table 1 presents the correlations between these variables. The obtained positive covariances indicate

Table 1. The statistical correlations between the QPPs' periods (p) and the host flare properties, i.e., duration (D) and energy (E).

Variables	Covariance	Pearson Correlation	Mutual Information
(p,D)	4.1×10^3	0.55	5.17
(p,E)	6.8×10^5	0.63	6

the dependency of the QPPs' periods on the flare parameters. However, the Pearson coefficient does not confirm a strong linear correlation. Figure 8 presents the scatter plots of the extracted periods versus the flare durations (top panel) and energies (bottom panel). The fan-shaped diagram of the top panel partially corresponds to the repeated values as multiple periods are detected in the PSDs of some QPPs (see e.g., black rectangles in the figure). It may also indicate the existence of another covariate influencing the dependency of pulsation periods on the flare durations. Nevertheless, no particular pattern is observed in the bottom panel.

We also calculate the non-linear correlations between the QPPs' periods and flare properties using the mutual information (Shannon 1948; Kreer 1957):

$$\mathcal{I}(p;f) = \int\int P(p,f) \log \frac{P(p,f)}{P(p)P(f)} dpdf, \tag{14}$$

where, $P(p)$ and $P(f)$ are marginal distributions of the periodicities and flare properties, respectively and $P(p,f)$ is the joint distribution. Following the Peng et al. (2005) routine, the mutual information is obtained a positive value (for both the duration and energy, see Table 1) which implies the existence of a missing parameter responsible for the observed non-constant (heterogeneous) variances. Although the measured correlations attest to the impacts of flaring events (reconnection regimes) on the production of QPPs, further observational or theoretical investigations are required to fully understand the involved processes and determine the parameters affecting the QPPs characteristics.

5. MODELING THE TIME SERIES OF QPPS

The study of real-world data and synthetic times series has a rich history that goes back over a hundred years. Time series analysis provides statistical information that sheds light on the underlying

generative mechanisms and may even result in prediction. To perform such analyses, numerous algorithms/tools have been developed which are mainly classified into two categories: frequency-based and time domain methods (Kantz & Schreiber 2003; Box et al. 2015; Shumway & Stoffer 2017; Chatfield & Xing 2019). A well-established paradigm of the first, e.g., the Lomb-Scargle periodogram, is introduced and implemented in Section 4. The second type operates based on correlation analysis. Here, we study the stochastic time series of both simulated and observational QPPs using a parametric time domain method. We apply an autoregressive integrated moving average (ARIMA) model to the non-stationary time series of QPPs and investigate their efficiency in characterizing the QPPs behavior.

The ARIMA models could adequately study processes with time varying mean values. These models, first, remove the non-stationarity by applying a backshift operator and then, fit either an autoregressive (AR), a moving average (MA), or a combination of these terms on the subject series (The Econometrics Toolbox User's Guide, MATLAB 2021). Both the AR and MA terms cope with the serial autocorrelations of a given time series and use the past observations and errors of the sample, respectively, to make predictions for the future values. A MA process of order q is defined as:

$$\begin{aligned} S_t &= Z_t + \theta_1 Z_{t-1} + \cdots + \theta_q Z_{t-q}, \\ &= (1 + \theta_1 B + \theta_2 B^2 + \cdots + \theta_q B^q) Z_t, \end{aligned} \tag{15}$$

where S_t is the sample value at time t, θ_i is the MA coefficient for $i = 1..q$, B is the backshift operator, and Z_t is a random value, generated from a Gaussian distribution (white noise). For the simplicity and without loss of generality, the expectation of the noise is assumed to be zero. Similarly, an AR process of order p is:

$$\begin{aligned} S_t &= Z_t + \phi_1 S_{t-1} + \cdots + \phi_p S_{t-p}, \\ &= Z_t + (\phi_1 B + \phi_2 B^2 + \cdots + \phi_p B^p) S_t, \end{aligned} \tag{16}$$

and ϕ_i $(i = 1..p)$ is AR coefficient.

Considering Equations (15) and (16), an ARIMA(p, d, q) process is defined as:

$$\left(1 - \sum_{i=1}^{p} \phi_i B^i\right)(1 - B)^d S_t = \left(1 + \sum_{j=1}^{q} \theta_j B^j\right) Z_t, \tag{17}$$

where d is the difference parameter and takes integer values. ARIMA models indicate the existence of short-memory autocorrelations in a system. A more general approach is to consider an additional $1/f$-type long-memory autocorrelation in the time series, for which the autoregressive fractionally integrated moving average (FARIMA or ARFIMA) models are applicable. The FARIMA models share the same representation of Equation (17) except that the difference parameter adopts non-integer values.

The application of the time domain methods has been of interest in astronomical studies in recent decades (e.g., Lazio et al. 2001; Stanislavsky et al. 2009; Templeton & Karovska 2009; Feigelson & Babu 2012; Kelly et al. 2014; Feigelson et al. 2018). In the following, we perform a parametric analysis on the registered energies of both simulated and observational flares of Figures 2 and 3, respectively. We use MATLAB's *EconometricModeler* toolbox to examine several choices of p, d, and q for both ARIMA and FARIMA models and discuss the results. The main motivation for fitting an ARIMA/FARIMA model to the time series of QPPs is to investigate the functionality of these methods in describing the quasi-oscillatory patterns of solar flares.

Figure 9 illustrates the autocorrelation function (ACF) and partial autocorrelation function (PACF) of the simulated QPPs. The lag number and the significant range are considered a quarter of the sample points and $\pm 2\sigma$, respectively. As seen in the figure, the ACF tails off gradually which is consistent with the existing trend in the time series. This indicates that a non-zero difference parameter is required for modeling. Moreover, a periodic-like pattern is observed in the ACF. The PACF also spikes strongly at lag 1. The autocorrelations provide some intuition about the order of parameters. However, the preferred values are those minimizing the Akaiki information criterion (AIC). AIC estimates the performance of an applied model on a given data sample. Further to this criterion, the residuals should be stationary and normally distributed. Figure 10 displays AICs for 900 examined ARIMA models. The minimum AIC corresponds to $p = 4, d = 1$, and $q = 5$. Strong

negative spikes are observed for models with $d = 2$ as a manifestation of overdifferencing. Figure 11 shows the simulated time series together with the ARIMA(4,1,5) model, and the residuals (left panels).

Even though the AIC has determined a decent model, an explicit investigation of residuals is still required to avoid possible mis-specifications. Besides stationarity, the residuals of a convenient ARIMA-type model should follow a Gaussian distribution with no correlations. In order to check whether these conditions are met, various tests are available e.g., Ljung-Box Q-test for autocorrelations, KS-test, KPSS test, Dickey–Fuller test, and etc. (see the Econometrics Toolbox User's Guide, MATLAB 2021, for a detailed review). We performed a detrended fluctuation analysis (DFA) on the residuals and obtained the Hurst exponent equal to 0.48 ± 0.01. We also investigated the existence of a unit root applying the mentioned tests and found that the residuals have similar characteristics to a white noise. The ACF of the residuals is shown in Figure 11 right panel.

Generally, quasi-periodic patterns are universal features that arise due to an underlying $1/\nu-$type process (Feigelson & Babu 2012). Such long-memory processes might be described with FARIMA models. The difference parameter of a stationary and invertible fractional ARIMA model lies in the range of $-1/2 < d_f < 1/2$, where d_f corresponds to the long-term dependency in the subject time series (Beran et al. 2013). There are several methods to measure the difference parameter of a FARIMA model such as performing a DFA (as $H = d_f + 1/2$), fitting a power law to either the gradual decay of ACF ($ACF(l) \propto l^{2d_f-1}$) or the Fourier PSD ($\mathcal{P}(\nu) \propto |\nu|^{-2d_f}$), or even performing a discrete wavelet transformation (Barkoulas & Baum 1997; Reisen et al. 2001). On the downside, different methods might not necessarily converge to the same result (see Feigelson & Babu 2012, section 11.9).

Applying a DFA, the Hurst exponent of the simulated QPPs is obtained 1.35 ± 0.01 which means that the time series is non-stationary, and leads to $d_f = 0.85$. Furthermore, we performed a power-law fit on the ACF of the QPPs and found $d_f = 0.75$. The obtained fractional differences imply that even though the process is mean reverting, the variance is infinite (Granger & Joyeux 1980). Beran et al. (2013) discussed cases for which both the fractional and non-fractional difference parameters are

required, namely, FARIMA$(p, d_{\rm total}, q)$ models with $d_{\rm total} = d + d_f$. One possible approach is to consider e.g., $d = 1$ and take the difference of the time series through $(1 - B)S_t$, then, compute d_f. Following this perspective, we obtain $d_f = -0.03$ which indicates a relatively weak long-term dependency.

We have also performed a similar analysis on the HXR emissions of the solar flare of Figure 3. The ACFs and PACFs relevant to each pass band are shown in Figure 12. Various choices of ARIMA parameters ($p, q = 1..20$, and $d = 1, 2$) are examined and their AICs are measured. The minimum AICs of the L, M1, M2, and H bands are achieved for ARIMA$(2, 1, 2)$, ARIMA$(4, 1, 3)$, ARIMA$(19, 1, 13)$ and ARIMA$(15, 1, 15)$, respectively. However, the residuals do not follow a Gaussian distribution in contrast with the initial assumption of Equation (17). Such violation might impact the maximum likelihood estimations performed for AIC calculation and model selection. Nonetheless, the obtained parameters might still be correct as the regression models could practically overcome the non-normality of residuals in many cases (see e.g., Knief & Forstmeier 2021). Figure 13 displays the registered emissions, ARIMA models and the residuals for each spectral band.

It seems that ARIMA models could conveniently characterize the time series of simulated flaring events. For the observational time series, more study is required to evaluate the influence of initial assumptions on model selection. In the next step, we would like to extend the study by considering a none-Gaussian noise in ARIMA-type models to adequately investigate their practicality in flare studies.

6. CONCLUSION

The scale-free nature of solar flare energies inspired the application of SOC models to investigate these phenomena. Despite the development of numerous MHD simulation models, less attention has been paid to the pre-existing CA models and their capabilities in simulating QPPs. In the present study, we took the idea of SOC together with the self-oscillatory processes (load/unload mechanism) into consideration and discussed that CA models could technically generate QPPs due to their intrinsic ability in reproducing repetitive reconnection regimes. Then, we reappraised the

well-known CA avalanche model of Lu & Hamilton and investigated the productivity of this model in evaluating QPPs' characteristics.

Applying the modified Lu & Hamilton model, we simulated 21,070 flaring events. We obtained that nearly 4% of these events last over 50 seconds, scaled with the HXT temporal resolution, which mostly includes the C-class flares and more energetic explosions (some B-class flares are also included in this list). The QPPs are found in 70% of these flares (565 out of 813). However, less than 1% of small-scale events ($D \leq 50$ seconds) exhibited quasi-periodic patterns. We applied the Lomb-Scargle periodogram to study the quasi-periodic patterns. The distribution of extracted periodicities follows a lognormal distribution with a global maximum of 29.29 ± 0.67 seconds which illustrates the most probable period for the simulated QPPs. The obtained lognormal behavior indicates the presence of a multiplicative mechanism (typifying the effect of independent varying parameters e.g., driving mechanism, number of unstable sites, released energies, etc.) due to which the system evolves. However, the stochastic and scale-free nature is preserved in the memory of the time series as an essential characteristic of the observational/simulated flaring events.

We observed that the CA models could practically produce a wide range of periodicities for QPPs. Moreover, the presence of multiple periods is observed in nearly 50% of simulated QPPs. According to our results, although there is a clear dependency between the QPPs' periods and the host flare durations, other covariates might also be involved that affect their relation. We obtained that the applied CA model adequately accomplishes simulating flares, QPPs, and their statistics. Moreover, we examined ARIMA-type models on the time series of observational and simulated QPPs. We observed that ARIMA models could describe the subject QPPs. However, further studies are required to address their utility in modeling flares and accompanying QPPs.

Acknowledgments: We acknowledge the use of data from the YLA. The authors gratefully thank Dr. Aki Takeda and Dr. Keiji Yoshimura from the YLA team for their kind response and preparation of the HXR time profiles. N.F. express her gratitude to the Iran National Science Foundation (INSF) for supporting this research under grant No. 99012824. The authors also gratefully acknowledge the anonymous Reviewer and statistics Editor for their constructive suggestions.

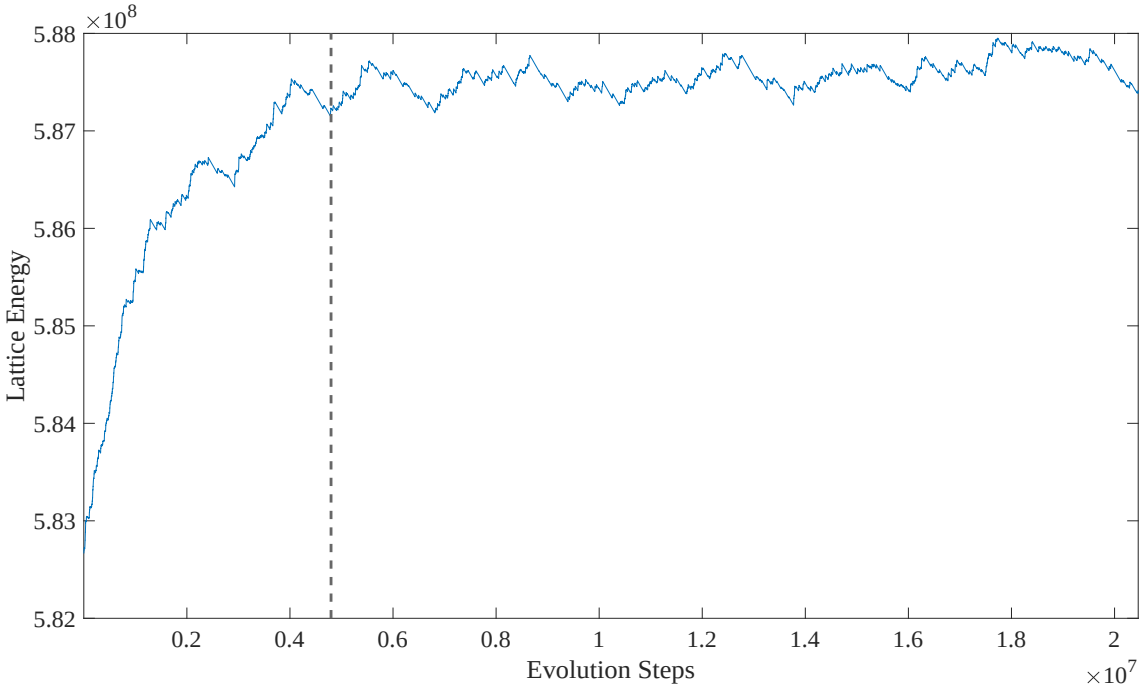


Figure 1. The evolution of the lattice energy in a magnetic vector potential lattice (with 2^{16} grids) during 200,000 driving steps. The initial lattice is constructed using uniformly distributed random numbers. After nearly 5 million evolution steps (dashed-line) the system reaches to an approximate stationary state. During the following steps, the driving mechanism injects energy into the system. Whereas, the avalanches emit energy.

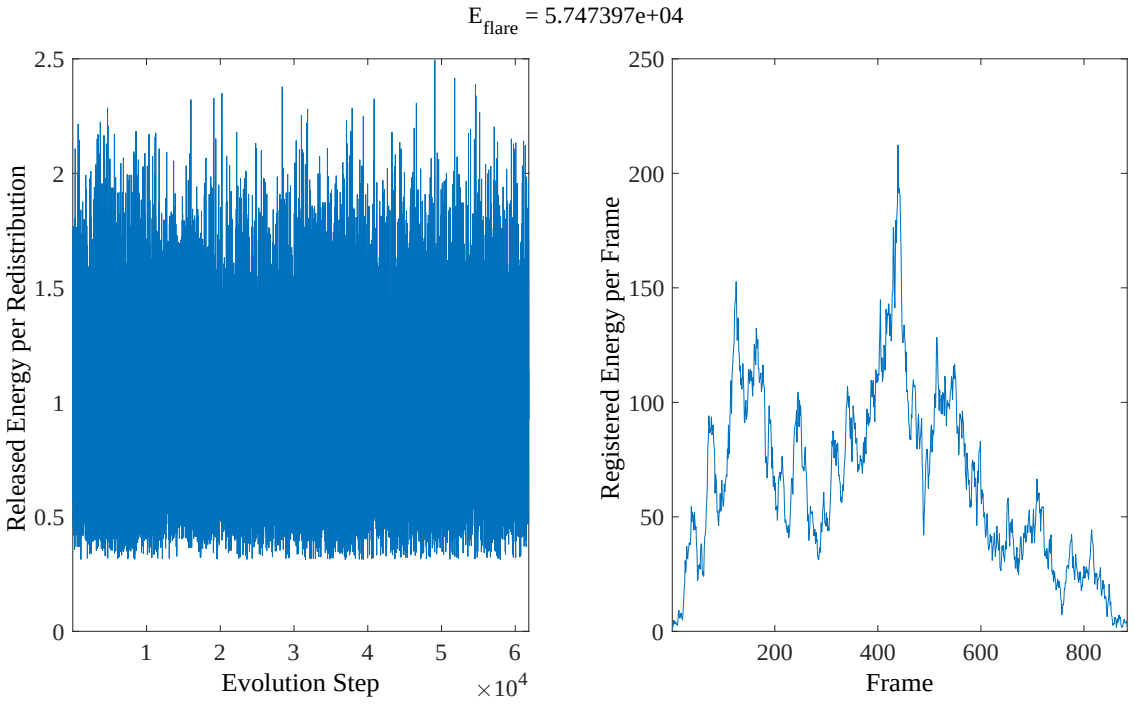


Figure 2. The registered energies of a typical simulated flare. During the subject flare, $61,834$ magnetic reconnections occurred (within 884 frames) leading to a total energy release of 5.74×10^4. The left panel shows the amount of energy released at each magnetic reconnection. The right panel illustrates the detected energies in successive frames.

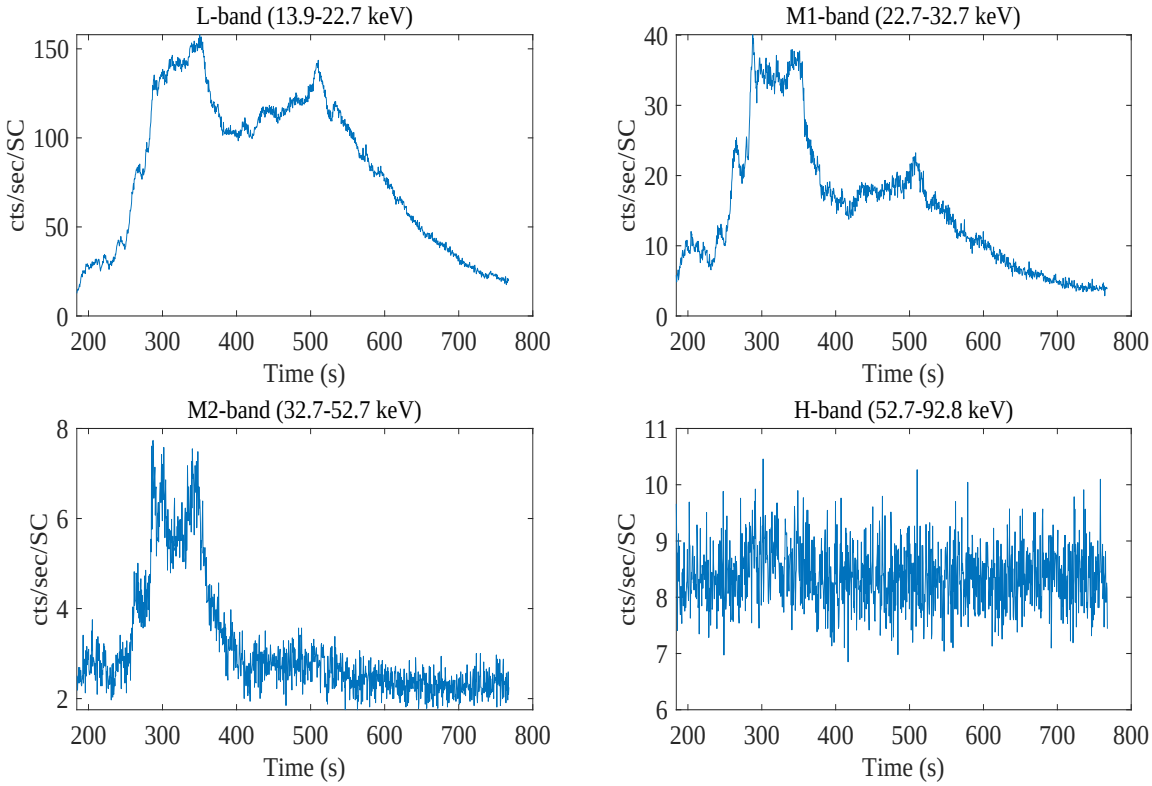


Figure 3. The HXR emissions of a solar flare registered by the Yohkoh satellite. The flaring event occurred at 17:09 March 1th, 1998 and was recorded by the HXT instrument in different energy bands (L: 13.9-22.7 keV, M1: 22.7-32.7 keV, M2: 32.7-52.7 keV, and H: 52.7-92.8 keV). The vertical axis represents the average count rate over the 64 spatially-modulated subcollimators (SC).

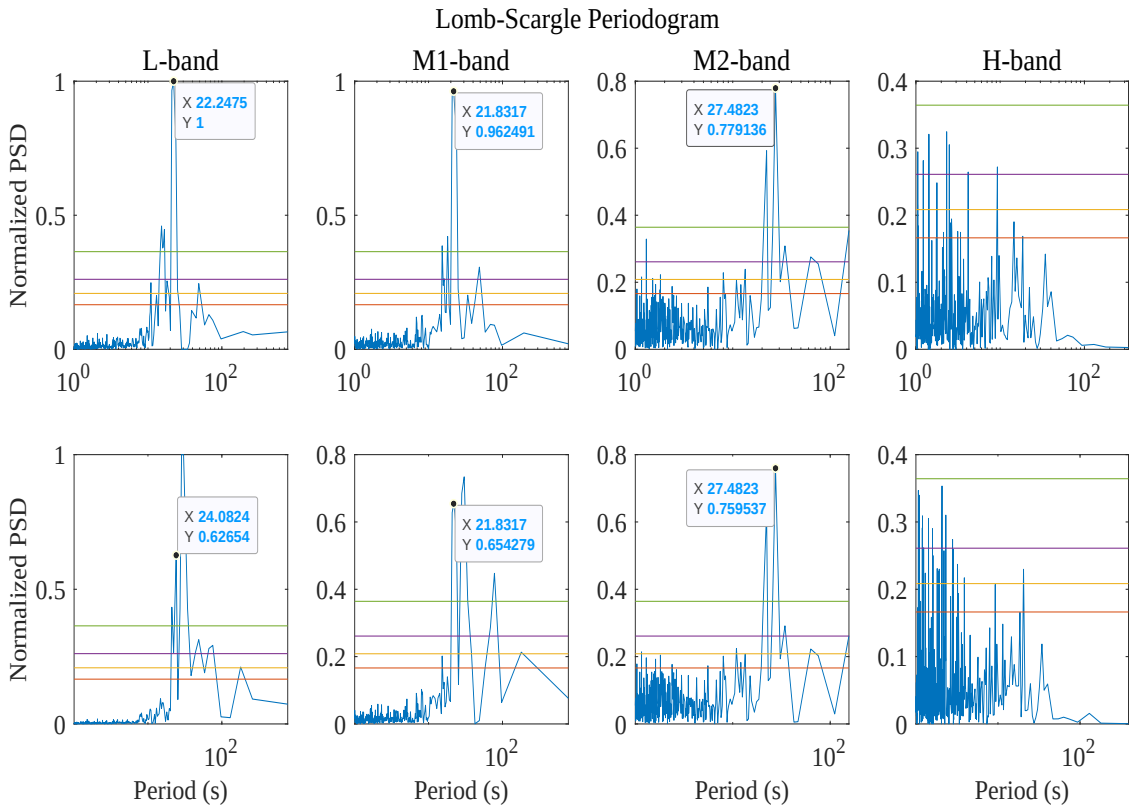


Figure 4. The normalized PSDs of the HXR emissions of a solar flare (Figure 3) registered in 4 different energy bands (L, M1, M2, and H) by the Yohkoh satellite. The frequency (period) components are extracted applying the Lomb-Scargle periodogram. The horizontal lines represent the FAP significance levels of $50, 10, 1$, and 0.01 percents displayed by the red, yellow, purple, and green colors, respectively. The top panels correspond to the smoothed time series (Equation 11) whilst the bottom panels are obtained for normalized time series (Equation 10).

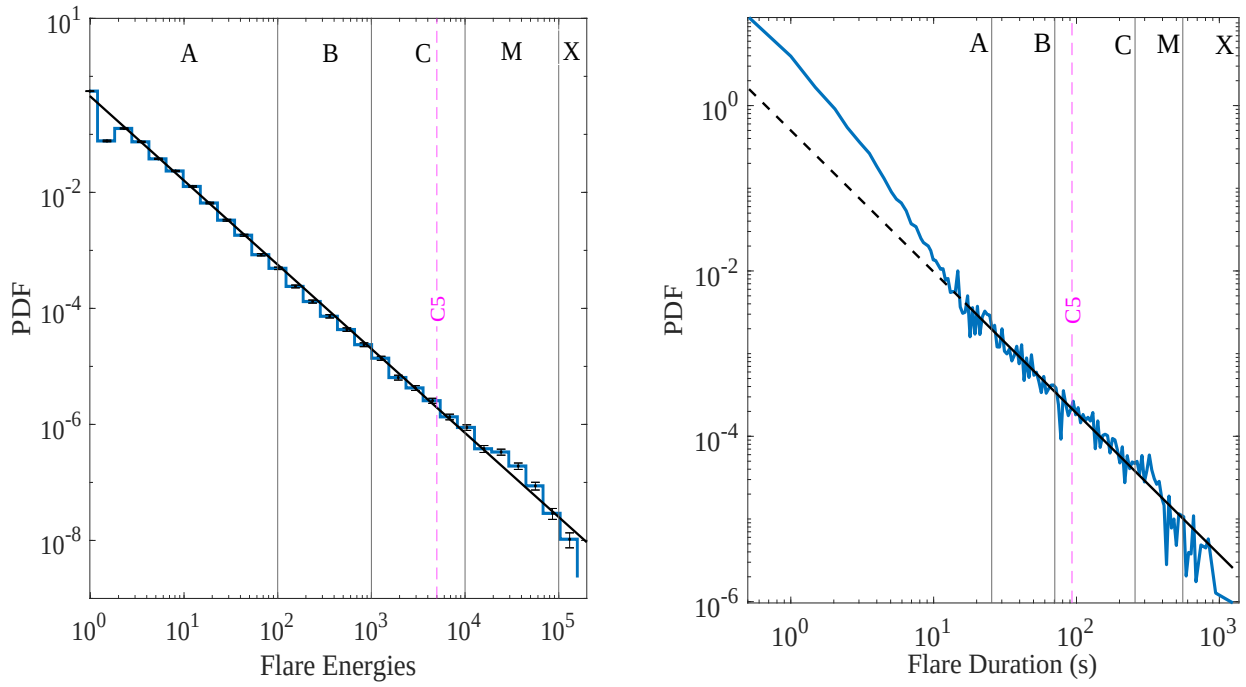


Figure 5. The PDFs of the flare energies (left panel) and durations (right panel) of simulated flares. Types of flares (A, B, C, M, and X) are identified based on the GOES classification system. A power-law function is fitted to both distributions. The power indices are 1.45 ± 0.02 and 1.71 ± 0.02, with the $p-$values of 0.98 and 0.90 for the left and right panels, respectively.

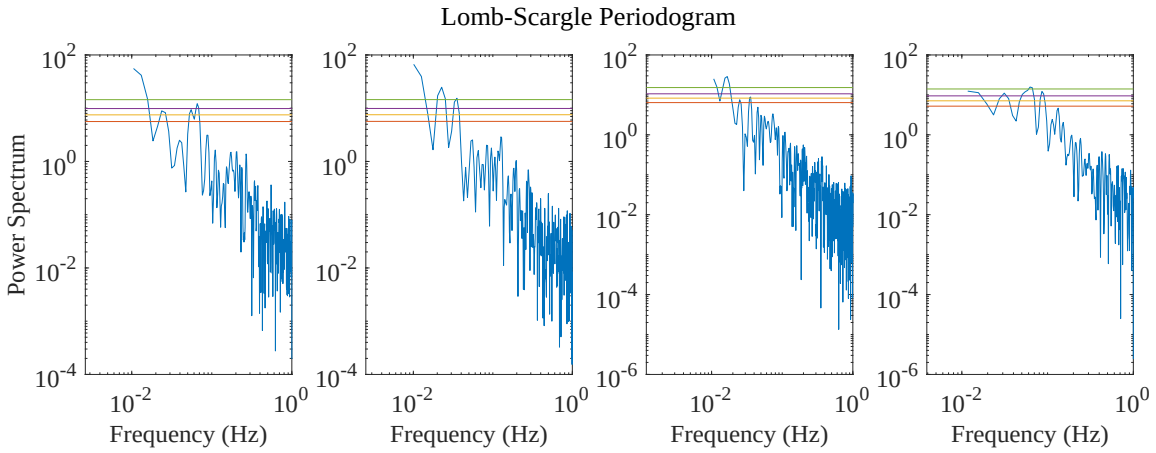


Figure 6. The log-frequency presentation of the PSDs for some of the simulated events.

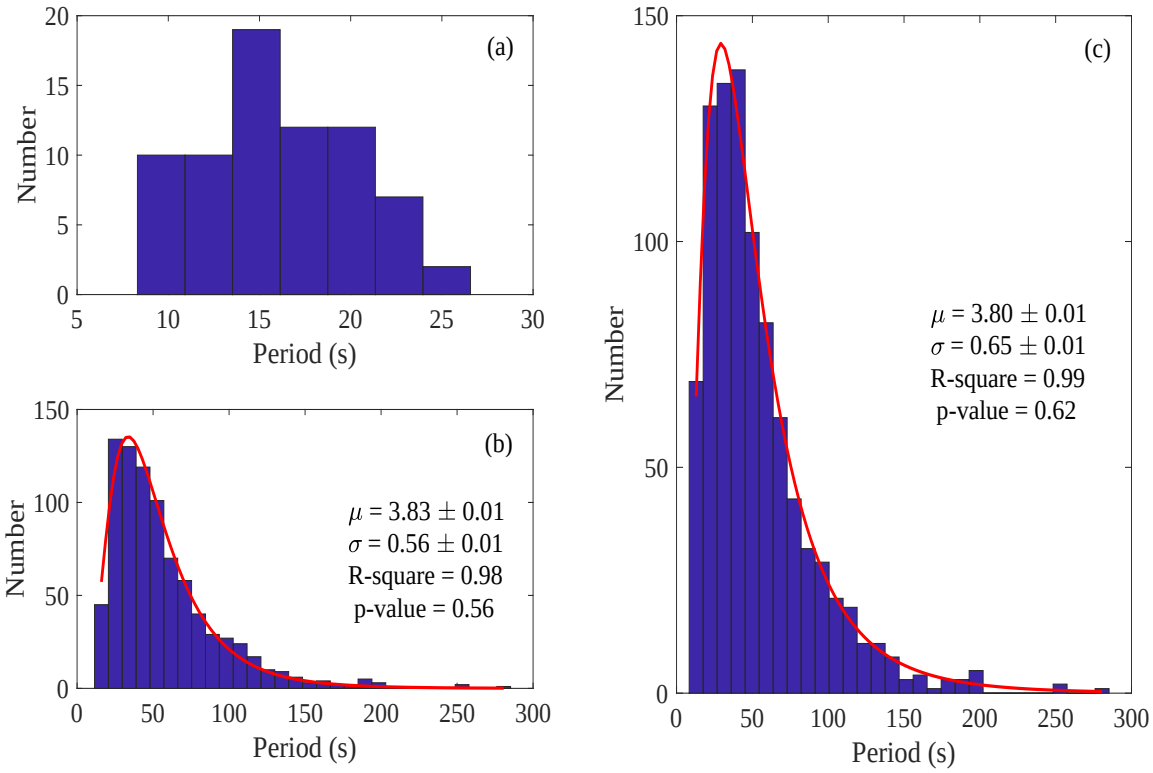


Figure 7. The histograms of the extracted periods for the simulated QPPs for: (a) $D \leq 50$ seconds and (b) $D > 50$ seconds. Panel (c) exhibits the number of collective periods of both regimes. The global maximums of the lognormal distributions are located at 33.66 ± 0.71 and 29.29 ± 0.67 seconds for panels (b) and (c), respectively. The goodness-of-fit is assessed applying both the R-squared statistics and KS-test.

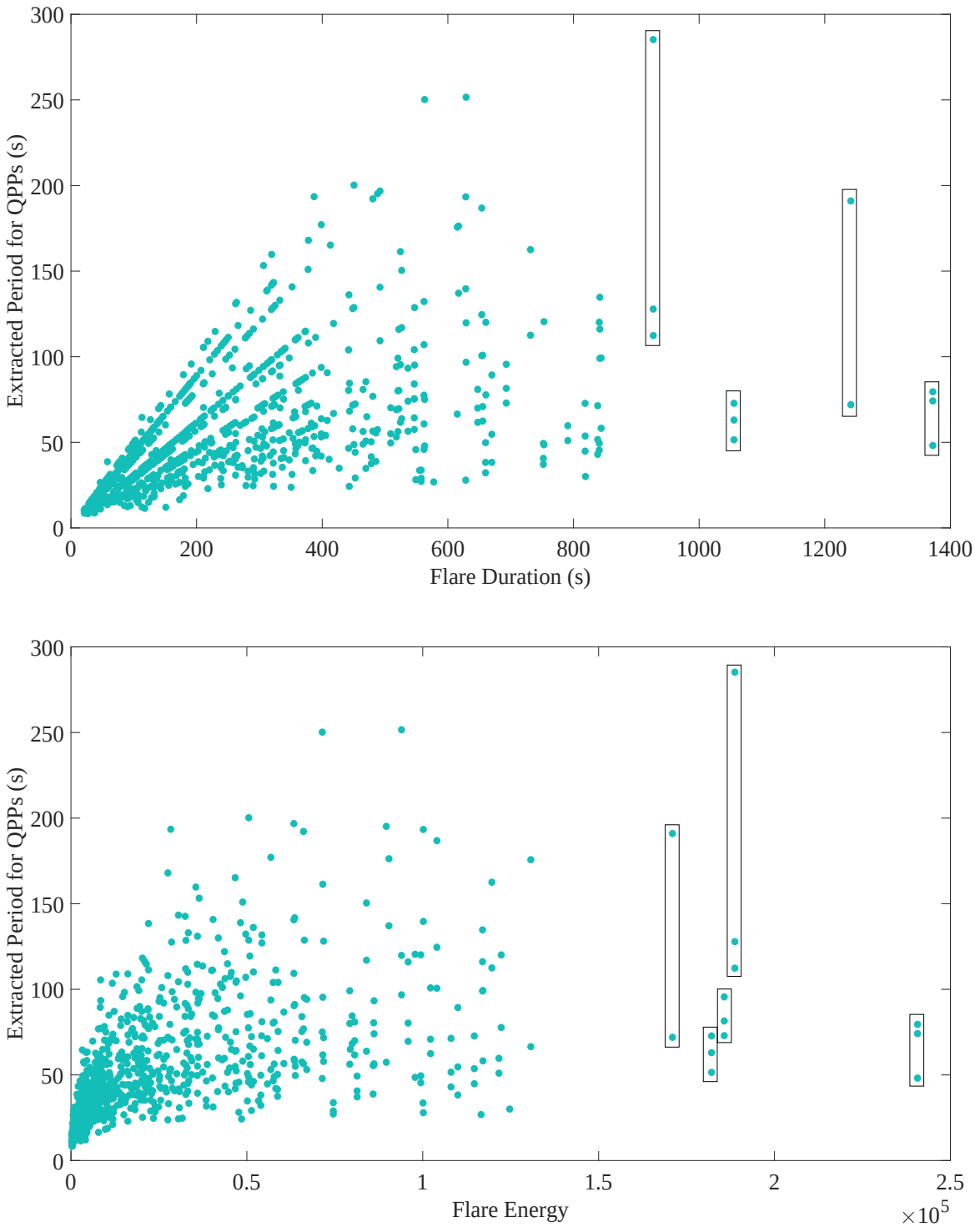


Figure 8. The scatter plots of the extracted periods for the simulated QPPs versus the host flare durations (top panel) and energies (bottom panel). The black rectangles illustrate some examples of the QPPs for which multiple periods are detected.

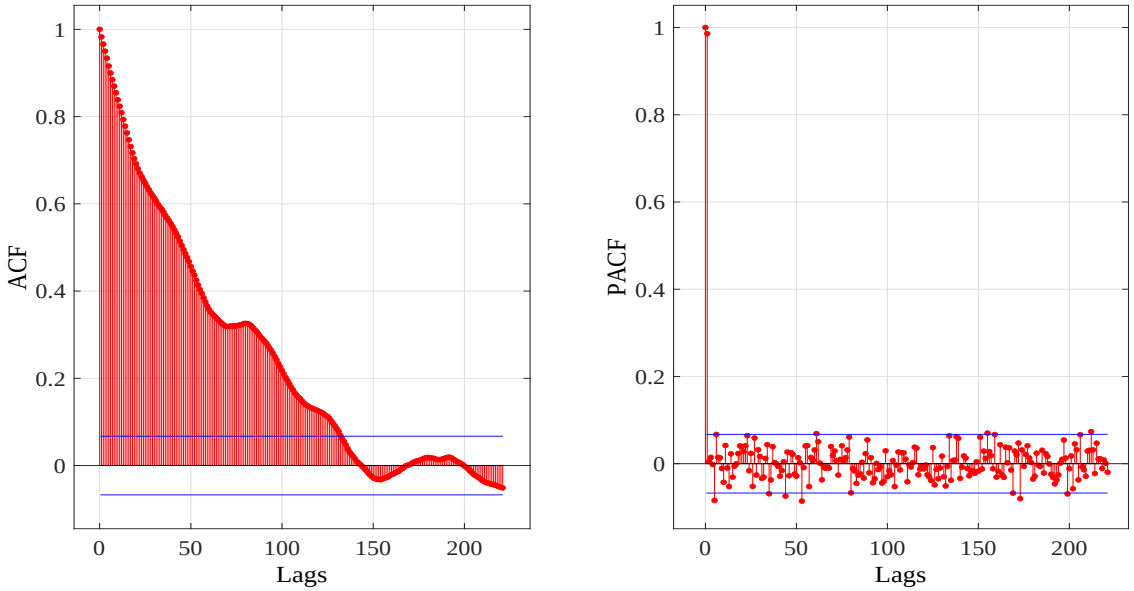


Figure 9. The ACF (left panel) and PACF (right panel) of the time series of the simulated QPPs presented in Figure 2.

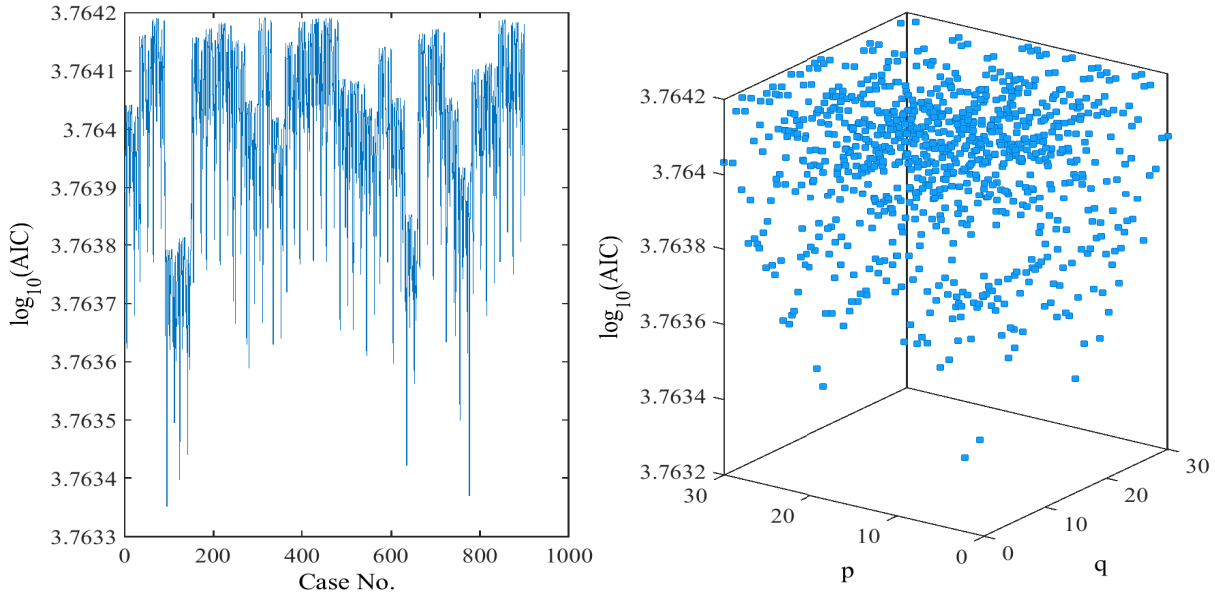


Figure 10. The AICs of 900 ARIMA models applied on the simulated QPPs of Figure 2 with $p, q = 1..30$, and $d = 1$.

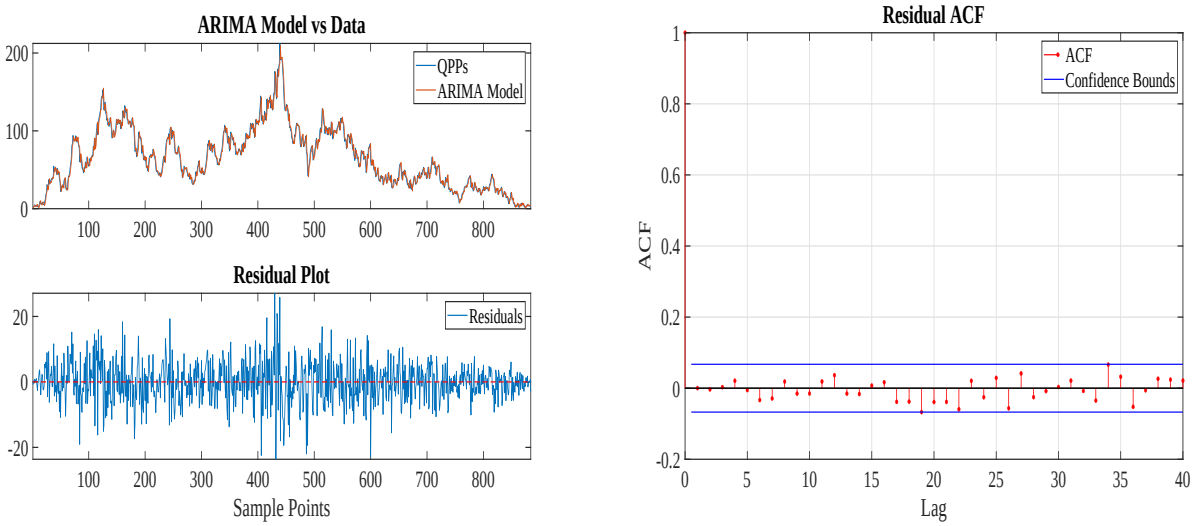


Figure 11. The simulated QPPs of Figure 2 vs the ARIMA(4,1,5) model (top left panel), the obtained residual (bottom left panel), and the ACF of the residuals (right panel).

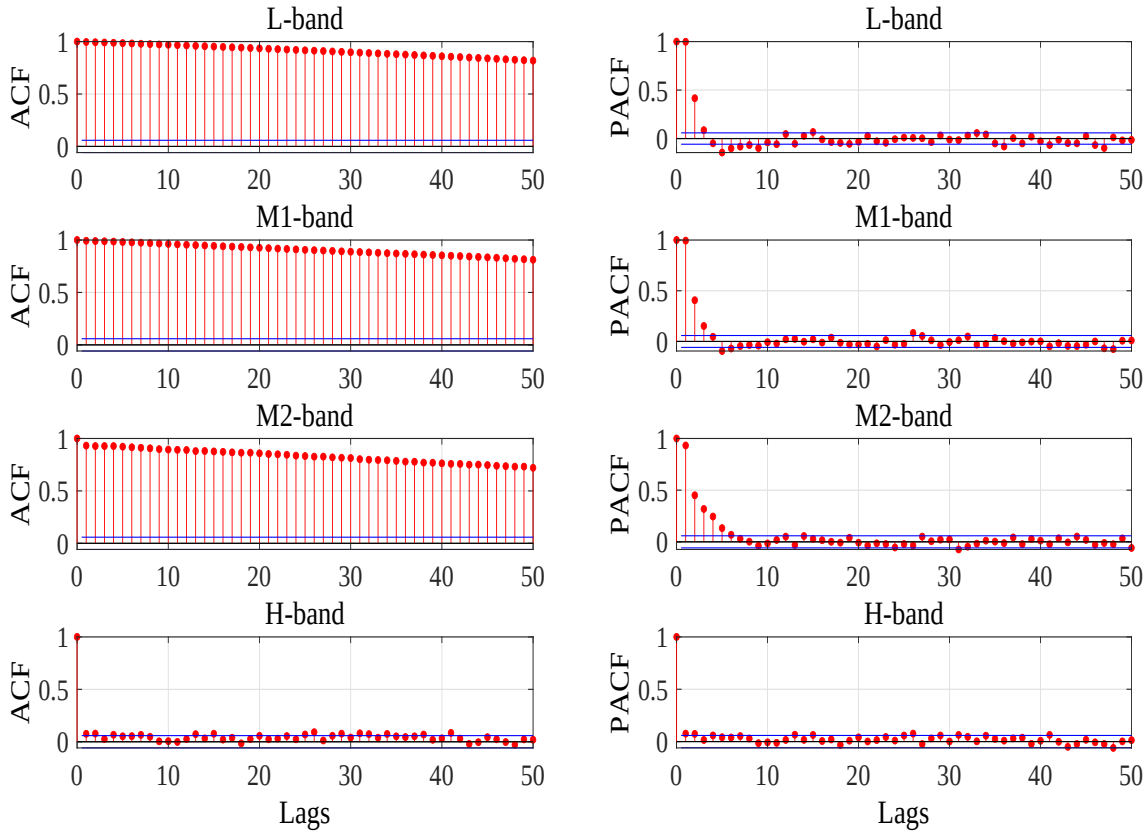


Figure 12. The ACFs and PACFs of the HXR emissions of the solar flare displayed in Figure 3.

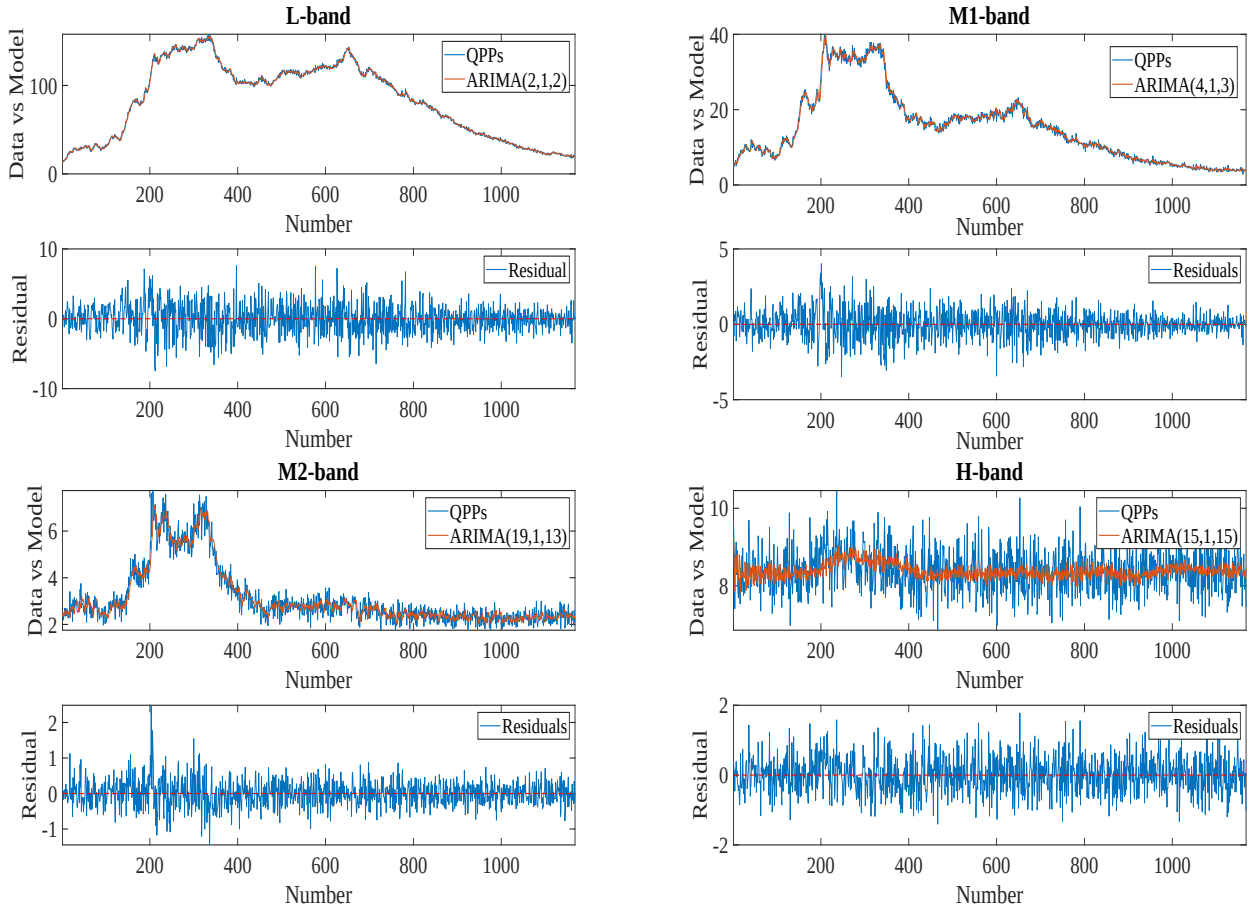


Figure 13. The HXR emissions of the solar flare of Figure 3 vs the selected ARIMA models and relevant residuals in four spectral bands of L, M1, M2, and H.

REFERENCES

Alipour, N., Mohammadi, F., & Safari, H. 2019, The Astrophysical Journal Supplement Series, 243, 20

Alipour, N., Safari, H., Verbeeck, C., et al. ????, Astronomy & Astrophysics

Aschwanden, M. 1987, Solar Physics, 111, 113

—. 2011, Self-Organized Criticality in Astrophysics (Springer-Verlag Berlin Heidelberg), XIV, 416

Bak, P., Tang, C., & Wiesenfeld, K. 1987, Physical Review Letters, 59, 381

Baluev, R. V. 2008, Monthly Notices of the Royal Astronomical Society, 385, 1279

Barkoulas, J. T., & Baum, C. F. 1997, Journal of Financial Research, 20, 355

Bazarghan, M., Safari, H., Innes, D. E., Karami, E., & Solanki, S. K. 2008, Astronomy and Astrophysics, 492, L13

Benz, A. O. 2017, Living Reviews in Solar Physics, 14, 1

Beran, J., Feng, Y., Ghosh, S., & Kulik, R. 2013, Long-Memory Processes: Probabilistic Properties and Statistical Methods, 1st edn. (Springer)

Berghmans, D., Auchère, F., Long, D., et al. 2021, Astronomy & Astrophysics, 656, L4

Biskamp, D. 2000, Magnetic Reconnection in Plasmas (Cambridge, UK: Cambridge University Press), 121–155

Box, G. E., Jenkins, G. M., Reinsel, G. C., & Ljung, G. M. 2015, Time series analysis: forecasting and control (John Wiley & Sons)

Carmichael, H. 1964, A Process for Flares, Vol. 50 (NASA), 451

Cenko, S., Butler, N., Ofek, E., et al. 2010, The Astronomical Journal, 140, 224

Charbonneau, P., McIntosh, S. W., Liu, H.-L., & Bogdan, T. J. 2001, Solar Physics, 203, 321

Chatfield, C., & Xing, H. 2019, The Analysis of Time Series: An Introduction with R, Chapman & Hall/CRC Texts in Statistical Science (CRC Press)

Chen, P., & Priest, E. 2006, Solar Physics, 238, 313

Chen, Y., Przybylski, D., Peter, H., et al. 2021, Astronomy & Astrophysics, 656, L7

Craig, I. J. D., & McClymont, A. N. 1991, The Astrophysical Journal Letters, 371, L41

De Moortel, I., & Nakariakov, V. M. 2012, Philosophical Transactions of the Royal Society A: Mathematical, Physical and Engineering Sciences, 370, 3193

Delisle, J.-B., Hara, N., & Ségransan, D. 2020a, Astronomy & Astrophysics, 635, A83

—. 2020b, Astronomy & Astrophysics, 638, A95

Dennis, B. R. 1985, in Progress in Solar Physics (Springer), 465–490

Dennis, B. R., Tolbert, A. K., Inglis, A., et al. 2017, The Astrophysical Journal, 836, 84

Dominique, M., Zhukov, A., Dolla, L., Inglis, A., & Lapenta, G. 2018, Solar Physics, 293, 1

Dănilă, B., Harko, T., & Mocanu, G. 2015, Monthly Notices of the Royal Astronomical Society, 453, 2982

Farhang, N., Safari, H., & Wheatland, M. S. 2018, The Astrophysical Journal, 859, 41

Farhang, N., Wheatland, M. S., & Safari, H. 2019, The Astrophysical Journal, 883, L20

Feigelson, E. D., & Babu, G. J. 2012, Modern statistical methods for astronomy: with R applications (Cambridge University Press)

Feigelson, E. D., Babu, G. J., & Caceres, G. A. 2018, Frontiers in Physics, 6, 80

Fletcher, L., Dennis, B. R., Hudson, H. S., et al. 2011, Space Sience Review, 159, 19

Forbes, T. G. 1991, Geophysical & Astrophysical Fluid Dynamics, 62, 15

Georgoulis, M. K., & Vlahos, L. 1998, Astronomy and Astrophysics, 336, 721

Gold, T., & Hoyle, F. 1960, Monthly Notices of the Royal Astronomical Society, 120, 89

Granger, C. W., & Joyeux, R. 1980, Journal of time series analysis, 1, 15

Gruber, D., Lachowicz, P., Bissaldi, E., et al. 2011, Astronomy & Astrophysics, 533, A61

Hayes, L. A., Gallagher, P. T., Dennis, B. R., et al. 2019, The Astrophysical Journal, 875, 33

—. 2016, The Astrophysical Journal Letters, 827, L30

Hirayama, T. 1974, Solar Physics, 34, 323

Hong, Z., Li, D., Zhang, M., et al. 2021, Solar Physics, 296, 1

Horne, J. H., & Baliunas, S. L. 1986, The Astrophysical Journal, 302, 757

Inglis, A., Ireland, J., Dennis, B., Hayes, L., & Gallagher, P. 2016, The Astrophysical Journal, 833, 284

Ireland, J., McAteer, R. J., & Inglis, A. R. 2014, The Astrophysical Journal, 798, 1

Isliker, H., Anastasiadis, A., Vassiliadis, D., & Vlahos, L. 1998, Astronomy and Astrophysics, 335, 1085

Kantz, H., & Schreiber, T. 2003, Nonlinear Time Series Analysis, 2nd edn. (Cambridge University Press), doi: 10.1017/CBO9780511755798

Kelly, B. C., Becker, A. C., Sobolewska, M., Siemiginowska, A., & Uttley, P. 2014, The Astrophysical Journal, 788, 33

Knief, U., & Forstmeier, W. 2021, Behavior Research Methods, 53, 2576

Kopp, R., & Pneuman, G. 1976, Solar Physics, 50, 85

Kreer, J. 1957, IRE Transactions on Information Theory, 3, 208

Lazio, T. J. W., Waltman, E. B., Ghigo, F. D., et al. 2001, The Astrophysical Journal Supplement Series, 136, 265

Li, D., Kolotkov, D., Nakariakov, V., Lu, L., & Ning, Z. 2020, The Astrophysical Journal, 888, 53

Lomb, N. R. 1976, Astrophysics and space science, 39, 447

Longcope, D. W. 1996, Solar Physics, 169, 91

Loureiro, N. F., & Uzdensky, D. A. 2016, Plasma Physics and Controlled Fusion, 58, 014021

Lu, E. T., & Hamilton, R. J. 1991, The Astrophysical Journal, 380, L89

Lu, L., Li, D., Ning, Z., Feng, L., & Gan, W. 2021, Solar Physics, 296, 1

MATLAB. 2021, Econometrics Toolbox User's Guide (R2021a) (The MathWorks, Inc.)

McLaughlin, J., Nakariakov, V., Dominique, M., Jelínek, P., & Takasao, S. 2018, Space Science Reviews, 214, 1

McLaughlin, J., Thurgood, J. O., & MacTaggart, D. 2012a, Astronomy & Astrophysics, 548, A98

McLaughlin, J., Verth, G., Fedun, V., & Erdélyi, R. 2012b, The Astrophysical Journal, 749, 30

Melnikov, V., Reznikova, V., Shibasaki, K., & Nakariakov, V. 2005, Astronomy & Astrophysics, 439, 727

Mendoza, M., Kaydul, A., de Arcangelis, L., Andrade, Jr., J. S., & Herrmann, H. J. 2014, Nature Communications, 5, 5035

Mitzenmacher, M. 2004, Internet mathematics, 1, 226

Morales, L., & Charbonneau, P. 2010, Nonlinear Processes in Geophysics, 17

Morales, L. F., & Charbonneau, P. 2008, Geophysical Research Letters, 35

Najafi, A., Darooneh, A. H., Gheibi, A., & Farhang, N. 2020, The Astrophysical Journal, 894, 66

Nakariakov, V., Anfinogentov, S., Storozhenko, A., et al. 2018, The Astrophysical Journal, 859, 154

Nakariakov, V., Arber, T., Ault, C., et al. 2004, Monthly Notices of the Royal Astronomical Society, 349, 705

Nakariakov, V., Foullon, C., Verwichte, E., & Young, N. 2006, Astronomy & Astrophysics, 452, 343

Nakariakov, V., & Melnikov, V. 2009, Space Science Reviews, 149, 119

Nakariakov, V., Melnikov, V., & Reznikova, V. 2003, Astronomy & Astrophysics, 412, L7

Nakariakov, V. M., & Verwichte, E. 2005, Living Reviews in Solar Physics, 2, 1

Nita, G. M., Gary, D. E., Lanzerotti, L. J., & Thomson, D. J. 2002, The Astrophysical Journal, 570, 423

Ofman, L., & Sui, L. 2006, The Astrophysical Journal Letters, 644, L149

Ogasawara, E., Martinez, L. C., De Oliveira, D., et al. 2010, in The 2010 International Joint Conference on Neural Networks (IJCNN), IEEE, 1–8

Panigrahi, S., & Behera, H. 2013, International Journal of Engineering and Advanced Technology, 3, 280

Parker, E. N. 1988, The Astrophysical Journal, 330, 474

Pauluhn, A., & Solanki, S. K. 2007, Astronomy & Astrophysics, 462, 311

Peng, H., Long, F., & Ding, C. 2005, IEEE Transactions on Pattern Analysis and Machine Intelligence, 27, 1226

Priest, E. 2014, Magnetohydrodynamics of the Sun (Cambridge, UK: Cambridge University Press)

Priest, E., & Forbes, T. 2000, Magnetic Reconnection: MHD Theory and Applications (Cambridge University Press)

Reisen, V., Abraham, B., & Lopes, S. 2001, Communications in Statistics-Simulation and Computation, 30, 787

Ruocco, G., Daraio, C., Folli, V., & Leonetti, M. 2017, Palgrave Communications, 3, 1

Sadeghi, M., & Safari, H. 2019, Iranian Journal of Physics Research, 12, 205

Saikia, S. B., Lueftinger, T., Folsom, C., et al. 2022, Astronomy & Astrophysics, 658, A16

Scargle, J. D. 1982, The Astrophysical Journal, 263, 835

Shannon, C. E. 1948, The Bell system technical journal, 27, 379

Shokri, Z., Alipour, N., Safari, H., et al. 2022, arXiv preprint arXiv:2201.04459

Shumway, R., & Stoffer, D. 2017, Time Series Analysis and Its Applications: With R Examples, Springer Texts in Statistics (Springer International Publishing)

Somov, B. V. 1991, Physical processes in solar flares, Vol. 172 (Springer Science & Business Media)

—. 2010, Physics-Uspekhi, 53, 954

Somov, B. V., & Kosugi, T. 1997, The Astrophysical Journal, 485, 859

Stanislavsky, A., Burnecki, K., Magdziarz, M., Weron, A., & Weron, K. 2009, The Astrophysical Journal, 693, 1877

Strugarek, A., Charbonneau, P., Joseph, R., & Pirot, D. 2014, Solar Physics, 289, 2993

Sturrock, P. 1968, in Symposium-International Astronomical Union, Vol. 35, Cambridge University Press, 471–479

Svestka, Z., & Cliver, E. 1992, in IAU Colloq. 133: Eruptive Solar Flares, Vol. 399, 1

Szaforz, Ż., & Tomczak, M. 2019, Advances in Space Research, 64, 1100

Tajfirouze, E., & Safari, H. 2012, ApJ, 744, 113. https://arxiv.org/abs/1112.4926

Takasao, S., & Shibata, K. 2016, The Astrophysical Journal, 823, 150

Tarnopolski, M., & Marchenko, V. 2021, The Astrophysical Journal, 911, 20

Templeton, M. R., & Karovska, M. 2009, The Astrophysical Journal, 691, 1470

Thurner, S., Klimek, P., & Hanel, R. 2018, Introduction to the Theory of Complex Systems (Oxford University Press), 446

Tokovinin, A. 2014, The Astronomical Journal, 147, 87

Upendran, V., & Tripathi, D. 2021, The Astrophysical Journal, 916, 59

Valdivia, J., Rogan, J., Munoz, V., et al. 2005, Advances in Space Research, 35, 961

Van Doorsselaere, T., De Groof, A., Zender, J., Berghmans, D., & Goossens, M. 2011, The Astrophysical Journal, 740, 90

Van Doorsselaere, T., Kupriyanova, E. G., & Yuan, D. 2016, Solar Physics, 291, 3143

VanderPlas, J. T. 2018, The Astrophysical Journal Supplement Series, 236, 16

Vio, R., Diaz-Trigo, M., & Andreani, P. 2013, Astronomy and Computing, 1, 5

Wheatland, M. 2001, Solar Physics, 203, 87

Wheatland, M. S. 2008, The Astrophysical Journal, 679, 1621

Wheatland, M. S., & Litvinenko, Y. E. 2001, The Astrophysical Journal, 557, 332

Zaitsev, V. V., & Stepanov, A. V. 2008, Physics-Uspekhi, 51, 1123

Zhang, G., Tu, Z.-L., & Wang, F. 2021, The Astrophysical Journal, 909, 83

Zimovets, I., McLaughlin, J., Srivastava, A., et al. 2021, Space Science Reviews, 217, 1